Solvent-Extraction and Langmuir-Adsorption-Based Transport in Chemically Functionalized Nanopore Membranes

Damian J. Odom, Lane A. Baker, and Charles R. Martin*

Department of Chemistry and Center for Research at the Bio/Nano Interface, University of Florida, Gainesville, Florida 32611-7200

Received: May 12, 2005; In Final Form: September 7, 2005

We have investigated the transport properties of nanopore alumina membranes that were rendered hydrophobic by functionalization with octadecyltrimethoxysilane (ODS). The pores in these ODS-modified membranes are so hydrophobic that they are not wetted by water. Nevertheless, nonionic molecules can be transported from an aqueous feed solution on one side of the membrane, through the dry nanopores, and into an aqueous receiver solution on the other side. The transport mechanism involves Langmuir-type adsorption of the permeating molecule onto the ODS layers lining the pore walls, followed by solid-state diffusion along these ODS layers; we have measured the diffusion coefficients associated with this transport process. We have also investigated the transport properties of membranes prepared by filling the ODS-modified pores with the water-immiscible (hydrophobic) liquid mineral oil. In this case the transport mechanism involves solvent extraction of the permeating molecule into the mineral oil subphase confined with the pores, followed by solution-based diffusion through this liquid subphase. Because of this different transport mechanism, the supported-liquid membranes show substantially better transport selectivity than the ODS-modified membranes that contain no liquid subphase.

Introduction

Synthetic nanopore membranes have been used for applications as diverse as ultrafiltration,[1,2] industrial gas separations,[3] filtrations,[4,5] and templates for the synthesis of nanomaterials.[6−8] Our group has had a long-standing interest in such nanopore membranes, more specifically, polymeric membranes prepared via the track-etch method,[9−11] and alumina nanopore membranes made through the anodization of aluminum.[12,13] We have developed a general method to synthesize nanomaterials within the pores of such membranes.[6,7,14−17] Because these membranes contain cylindrical pores, this method yields correspondingly cylindrical nanowires or nanotubes prepared by any of a variety of synthetic methods within the pores.[18]

We are especially interested in nanotube-containing membranes prepared by the template method. For example, we have shown that gold nanotubes can be deposited within the pores of polymeric templates and that the inside diameters of these nanotubes can be of molecular dimensions (<1 nm).[19] Furthermore, the inside walls of the Au nanotubes can be chemically or biochemically functionalized, and this dramatically changes the transport properties of the nanotube membrane.[20−25] For example, Au nanotube membranes functionalized with hydrophobic thiols selectively transport hydrophobic molecules.[26]

The hydrophobic-thiol-functionalized Au nanotube membranes proved especially interesting because we found that after functionalization the Au nanotubes would no long fill with water. Nevertheless, nonionic molecules could be transported from an aqueous feed solution on one side of the membrane, through the dry nanotubes, and into an aqueous receiver solution on the other side.[27,28] We suggested that the transport mechanism entailed solvent extraction of the permeating molecule from the aqueous feed solution onto the hydrophobic thiol layers lining the nanotube walls, followed by solid-state diffusion along these thiol layers.[27] However, in that preliminary report, there were no data to confirm this proposed transport model.

We have since turned our attention to nanopore alumina membranes rendered hydrophobic by functionalization with octadecyltrimethoxysilane (ODS). In analogy to the hydrophobic Au nanotube membranes,[27] the pores in the ODS-modified aluminas are no longer wetted by water. Nevertheless, again, nonionic molecules could be transported from an aqueous feed solution on one side of the membrane into an aqueous receiver solution on the other side. We have found, however, that these ODS-modified membranes take up the permeating molecule from the aqueous feed solution via a Langmuir-adsorption process and not via solvent extraction, as suggested previously.[27] However, in agreement with our earlier work, we have found that transport occurs through the membrane via solid-state diffusion along the ODS layers lining the pore walls, and we have measured the diffusion coefficients associated with this transport process.

In solution, diffusion coefficients scale inversely with the radius of the diffusing molecule.[29] In contrast, we have found that the solid-state diffusion coefficients in the ODS-modified membranes scale inversely with the surface area of the molecule. This functional dependence seriously impairs the transport selectivity that can be obtained from these membranes. For this reason, we have also investigated supported-liquid membranes[30,31] in which the ODS-modified nanopores are filled with the hydrophobic liquid mineral oil. In this case, the membrane takes up the permeating molecule via solvent extraction, and transport occurs by solution-based diffusion in the mineral oil subphase confined within the pores. These supported-liquid membranes show substantially better transport selectivity than

* Corresponding Author. E-mail: crmartin@chem.ufl.edu.

10.1021/jp0524983 CCC: $30.25
Published on Web 10/15/2005

the ODS-modified membranes that contain no liquid subphase. The results of these investigations are reported here.

Experimental Section

Materials. Alumina Anodisc 47 filter membranes (60 μm thick, 47 mm diameter, and ~50% porosity) were obtained from Whatman. Two different versions of these membranes were used. The first contained nominally cylindrical pores with a pore diameter, as specified by the supplier, of 200 nm; these are designated here as the CP200 membranes. The second type of membrane contained cylindrical pores through most of the membrane's thickness, but these pores branched into nominally 20-nm-diameter pores at one face of the membrane. The branched-pore region of the membrane accounts for ~1 μm of the total membrane thickness.[32] These branched pore membranes are designated here as BP20 membranes.

$NiSO_4$, phenol, *p*-cresol, 2,4-dimethylphenol, 2,4,6-trimethylphenol, tetrahydrofuran, hexane, light mineral oil, kerosene, absolute alcohol, sodium acetate, NaH_2PO_4, and hexagonal polystyrene weighing boats were used as received from Fisher Scientific. Octadecyltrimethoxysilane was obtained from Gelest and used as received. Extra-fast-setting epoxy was obtained from Cole Parmer and used as instructed. Purified water was prepared by circulating house-distilled water through a Millipore Milli-Q water purification system.

Preparation of the Octadecyltrimethoxysilane (ODS) Modified Membranes. We have previously shown that silanes can be covalently attached to the pore walls and membrane faces of the alumina membranes studied here.[26,33] Before modification with ODS, the alumina membranes were cleaned by sequentially rinsing with water, tetrahydrofuran, and acetone. ODS modification was accomplished by immersing the membrane into a solution prepared by mixing 2 mL of the ODS with 15 mL of absolute alcohol and 1 mL of a 50 mM, pH = 5.1 sodium acetate buffer. Membranes were treated in this solution for 1 h with agitation, rinsed with absolute alcohol, and placed in an oven overnight at 80 °C.

Preparation of the Membrane Samples. Transport data were obtained on three different classes of membrane: 1. ODS-modified CP200 and BP20 membranes. 2. As-received CP200 and BP20 membranes. We use the term untreated to describe these membranes. 3. Supported-liquid membranes[30,31] where the pores in an ODS-modified BP20 membrane were filled with light mineral oil.

For the untreated and ODS-modified membranes (no mineral oil), the membrane samples were assembled as described previously, and then clamped between the two halves of a U-tube permeation cell.[26,27] The feed and receiver half-cells both contained 15 mL of solution, and the membrane assembly exposed 0.71 cm^2 of membrane area to these solutions. The feed solution contained a known concentration of the desired permeating molecule or ion (dissolved in 50 mM, pH = 7 NaH_2PO_4 buffer); buffer was placed in the receiver half-cell. The U-tube cell was placed into a constant-temperature bath at 25 ± 1 °C, and both half-cell solutions were vigorously stirred during the transport experiments.

The membrane assembly discussed above could not be used for the supported-liquid membranes. This is because this assembly uses Parafilm to secure the membrane sample,[26] and Parafilm is not chemically compatible with mineral oil. A polystyrene-based membrane assembly was used instead. A 0.97 cm^2 hole was punched into a section of polystyrene that was cut from the bottom of a weighing boat (~280 μm thick). Epoxy glue was applied around the hole, and the alumina membrane sample was carefully potted in the epoxy such that the membrane completely covered the hole. The membrane pores were then loaded with mineral oil by simply pipetting the oil onto the membrane surface. The membranes were then mounted in the U-tube cell, and the cell was thermostated and stirred during the transport experiments.

Transport Experiments. The transport data for all membrane samples were processed via "flux" plots, moles of permeating species transported across the membrane vs time. The quantity of permeating species transported was determined by periodically measuring the UV absorbance of the receiver solution. The following wavelengths were used: Ni^{2+}, 385 nm; phenol, 268 nm; *p*-cresol, 276 nm; 2,4-dimethylphenol, 276 nm; and 2,4,6-trimethylphenol, 277 nm. An Agilent 8453 instrument, with Agilent ChemStation software, was used for these measurements. Calibration curves were used to convert the measured absorbance into the concentration of permeating species in the receiver half-cell. All flux plots presented here represent averages of three replicate experiments on the same membrane sample.

Measurement of Partition Coefficients. As we will see, the rate and selectivity of transport obtained for the supported-liquid membranes is related to the partition coefficient (K_p) for the permeating species between the aqueous feed solution and the mineral oil confined within the pores. For this reason, mineral-oil/water K_p values were obtained for the permeating molecules phenol, *p*-cresol, 2,4-dimethylphenol, and 2,4,6-trimethylphenol. This was accomplished via solvent-extraction by using aqueous solutions that were initially 2 mM in the desired permeating molecule. A known volume of this aqueous solution (V_a) was added to a 20 mL vial, a volume V_o of mineral oil was then added, and the vial was sealed with a screw-on lid. The vial was shaken manually for ~1 h, and the phases were allowed to separate. The equilibrium concentration of the molecule in the aqueous phase ($C_{eq,a}$) was then determined by UV absorbance. The equilibrium concentration in the organic phase ($C_{eq,o}$) was obtained by difference.

If the initial 2 mM concentration of the molecule in the aqueous phase is defined as ($C_{in,a}$), then conservation of matter requires that

$$V_a C_{in,a} = V_a C_{eq,a} + V_o C_{eq,o} \quad (1)$$

Dividing both sides of eq 1 by V_a and $C_{eq,a}$ and noting that $K_p = C_{eq,o}/C_{eq,a}$ yields[34,35]

$$\left(\frac{C_{in,a}}{C_{eq,a}}\right) - 1 = K_p\left(\frac{V_o}{V_a}\right) \quad (2)$$

According to eq 2, a plot of $[(C_{in,a}/C_{eq,a}) - 1]$ vs V_o/V_a should be linear with slope = K_p.[27,36] In our experiments, the sum of V_a and V_o was always 20 mL, and V_a was varied from 5 to 19 mL.

Contact Angle Measurements. A Tantec CAM-Micro contact meter was used to determine surface contact angles for the untreated and ODS-modified membranes by using the half-angle technique, as described in the user's manual. Water droplets 10 μL in size were used, and each reported contact angle represents the average of four measurements.

Molecular Models. Models for the permeating molecules phenol, *p*-cresol, 2,4-dimethylphenol, and 2,4,6-trimethylphenol were calculated from energy-minimized structures using HyperChem (HyperCube) molecular-modeling software. The van der Waals surface area of each molecule was then calculated using QSAR protocols. The radius of each molecule was

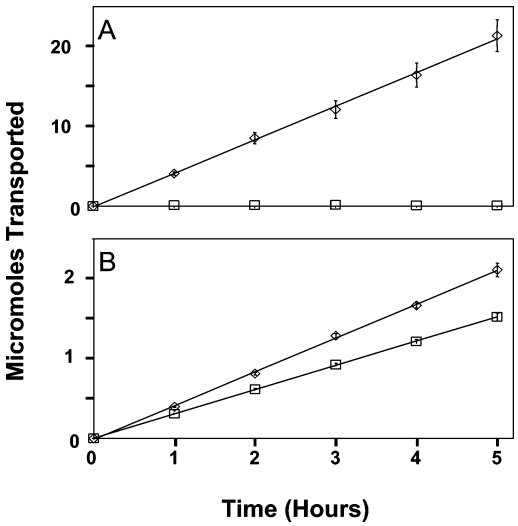

Figure 1. Flux plots. (A) Ni^{2+} transport in an untreated (◇) and ODS-modified (□) CP200 membrane. The concentration of Ni^{2+} in the feed solution was 100 mM. (B) DMP transport in an untreated (◇) and ODS-modified (□) CP200 membrane. The concentration of the DMP in the feed solution was 10 mM.

calculated from the surface area assuming that the molecule is disk shaped. This calculation requires values for the thicknesses of these disk-shaped molecules. On the basis of the molecular models, we used thicknesses of 0.34 nm for phenol and 0.42 nm for the methylated phenols.

Results and Discussion

Transport of Ni^{2+} and 2,4-Dimethylphenol Through Untreated and ODS-Modified Membranes. Figure 1A shows flux plots for Ni^{2+} transport across untreated and ODS-modified CP200 membranes. For the untreated membrane, the plot is linear (upper curve in Figure 1A), and the flux of Ni^{2+} across the membrane (58 ± 3 μmol cm^{-2} h^{-1}) was obtained from the slope. In contrast, no evidence for Ni^{2+} transport through the ODS-treatment was observed (lower plot in Figure 1A), even after permeation times as long as 24 h (data not shown). Contact-angle measurements were used to explain this difference between the transport properties of the untreated and ODS-modified membranes.

A contact angle could not be measured for the untreated membrane because the water droplet rapidly spread across the membrane surface and filled the pores. In contrast, the contact angle of water on the surface of an ODS-modified membrane was 120°, with no evidence of pore filling. This lack of pore wetting explains why the ODS-modified membrane is impermeable to Ni^{2+}; i.e., because the aqueous feed solution is denied access to the pores in the membrane, and the feed and receiver solutions are isolated from each other by this very hydrophobic membrane. Analogous results were obtained for gold nanotube membranes that had been modified with hydrophobic hexadecyl thiol.[27]

Figure 1B shows the analogous flux plots for 2,4-dimethylphenol (DMP) across the untreated and ODS-modified CP200 membranes. Because of its lower extinction coefficient, the feed concentration used in the Ni^{2+} experiments (Figure 1A) was an order of magnitude higher than those in the DMP experiments (Figure 1B). This concentration difference accounts for the lower flux of DMP in the untreated membrane (5.94 ± 0.07 μmol cm^{-2} h^{-1}). However, when the fluxes are corrected for this feed-concentration difference, the Ni^{2+} and DMP fluxes in the untreated CP200 membranes are identical. This indicates the aqueous-phase diffusion coefficients for these two species do not differ significantly.

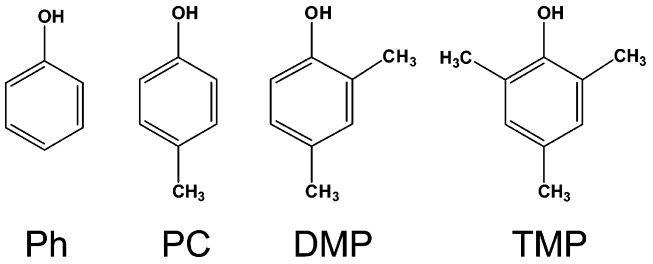

Figure 2. Chemical structures for the homologous series of permeate molecules.

The key difference between the Ni^{2+} and DMP transport data is that, while Ni^{2+} is not transported across the ODS-modified membrane (Figure 1A), DMP is transported across this membrane (Figure 1B). Indeed, the DMP flux across the ODS-modified membrane is only 28% lower than flux of DMP across the untreated membrane. The contact angle and transport data have shown that water and 100 mM aqueous Ni^{2+} solution do not wet the pores of the ODS-modified membrane. One possible explanation for the observed DMP flux across the ODS-modified membrane is that 10 mM DMP alters the properties of this aqueous solution such that this solution is able to wet the pores of the membrane.

To investigate this possibility, transport experiments were done with an ODS-modified CP200 membrane by using a feed solution that was 10 mM in DMP and 100 mM in Ni^{2+}. If DMP promoted pore flooding, then a measurable flux of Ni^{2+} would be observed. However, the flux of Ni^{2+} across the ODS-modified membrane using this feed solution was again zero. Furthermore, the DMP flux from this feed solution was identical to that obtained from the feed solution that contained only 10 mM DMP. These results show that DMP is being transported across the ODS-modified membrane even though the pores are not wetted by the aqueous feed solution. These data clearly show that the transport mechanism for DMP in the ODS-modified membrane is different than the solution-diffusion mechanism operative in the water-filled pores of the untreated membrane.

Transport of a Homologous Series of Permeating Molecules. At least two possible models can be proposed for DMP transport across the ODS-modified membrane. The first entails evaporation of the DMP from the feed solution at the membrane–solution interface, vapor-phase transport of the DMP through the dry pores, and redissolution of the DMP into the receiver solution. We call this the vapor-phase transport model. The second model entails hydrophobic-effect-driven partitioning of the hydrophobic DMP from the feed solution into the hydrophobic ODS-modified membrane, transport of DMP via diffusion in (or on) the ODS films lining the pore walls, and back partitioning of the DMP into the receiver solution. We call this the hydrophobic-partitioning/diffusion model. For both of these models, the driving force for transport is the difference in chemical potential of DMP between the feed solution, where it has a finite (and for these experiments constant) concentration, and the receiver solution where, for these experiments, its concentration is always effectively zero.

Transport experiments on a homologous series of permeating molecules can be used to distinguish between these two models. The homologous series used consisted of phenol (Ph), *p*-cresol (PC), DMP, and 2,4,6-trimethylphenol (TMP) (Figure 2). If the vapor-phase transport model is operative, flux will decrease with the increasing molecular weight of the molecules in this homologous series because vapor pressure deceases with

TABLE 1: Fluxes of the Various Permeating Molecules in the Untreated BP20 and CP200 Membranes; Feed Concentration Was 2 mM.

permeating molecule	flux (μmol cm^{-2} h^{-1})	
	BP20	CP200
Ph	0.283 ± 0.005	1.45 ± 0.07
PC	0.26 ± 0.02	1.38 ± 0.08
DMP	0.256 ± 0.004	1.38 ± 0.08
TMP	0.228 ± 0.004	1.27 ± 0.07

increasing molecular weight.[37] In contrast, if the hydrophobic-partitioning/diffusion model is operative, flux will increase with increasing molecular weight of the molecules in this homologous series. This is because the partition coefficients for these molecules from the aqueous feed solution and into the hydrophobic ODS-modified membrane will increase with increasing molecular weight of the permeating molecule.[38]

Permeation experiments with this homologous series were first performed on untreated CP200 and BP20 membranes using 2 mM aqueous feed solutions of the permeating molecules. For both membranes, the resulting flux plots were linear, and the fluxes of the various permeating molecules were calculated from the slopes (Table 1). The fluxes across the untreated CP200 membrane were higher than the fluxes across the untreated BP20 membrane, indicating, as expected, that the smaller pore diameter in the branched-pore layer restricts transport across the BP20 membrane. For each membrane, there was little to no difference in the Ph, PC, and DMP fluxes (Table 1). This is because the pores in these untreated membranes are flooded with the aqueous feed solution, and the differences in the diffusion coefficients for these molecules are too small to be detected via these transport experiments.

Figure 3 shows flux plots for the homologous series across the ODS-modified BP20 and CP200 membranes. In contrast to the untreated membranes, the fluxes for the various permeating molecules are not the same, and in general, flux increases with increasing molecular weight of the permeating molecule. As noted above, this trend is consistent with the hydrophobic-partitioning/diffusion model and inconsistent with the vapor-phase transport model. The fluxes obtained from the slopes of the flux plots are shown in Table 2.

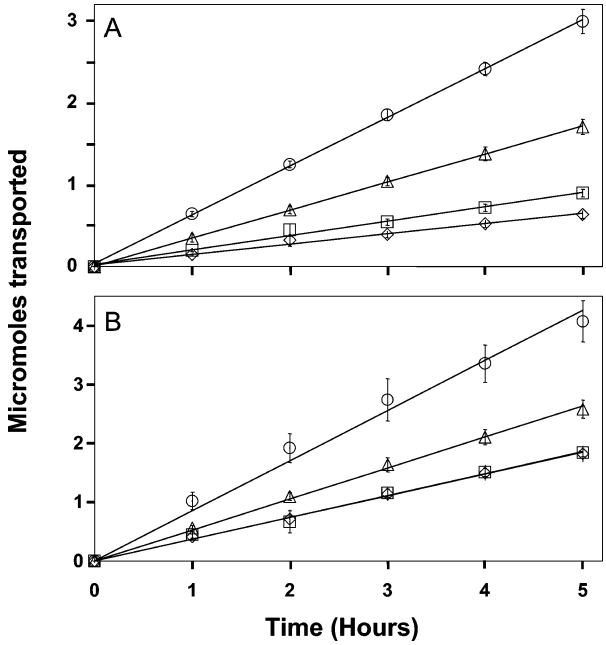

Figure 3. Flux plots for the homologous series of permeating molecules, (○) TMP, (△) DMP, (□) PC, (◇) Ph. Concentration in the feed solution was 2 mM. (A) ODS-modified BP20 membrane. (B) ODS-modified CP200 membrane.

TABLE 2: Fluxes and Transport Selectivity Coefficients (α_t) for the Various Permeating Molecules in the ODS-modified BP20 and CP200 Membranes; Feed Concentration Was 2 mM.

permeating molecule	ODS-modified BP20		ODS-modified CP200	
	flux (μmol cm^{-2} h^{-1})	α_t	flux (μmol cm^{-2} h^{-1})	α_t
Ph	0.176 ± 0.009	1	0.51 ± 0.01	1
PC	0.25 ± 0.01	1.4	0.52 ± 0.02	1
DMP	0.480 ± 0.002	2.73	0.72 ± 0.01	1.4
TMP	0.838 ± 0.009	4.76	1.13 ± 0.05	2.2

The transport selectivity of each membrane was quantified by taking a ratio of the fluxes of the various permeating molecules in the membrane to the phenol flux in that membrane. These ratios provide a family of selectivity coefficients (α_t, where the subscript t denotes transport selectivity) (Table 2). Phenol was chosen as the reference flux for these selectivity coefficients because it showed the lowest flux in each membrane, making the α_t values greater than or equal to unity. The selectivity data for the ODS-modified membranes are also consistent with the hydrophobic-partitioning/diffusion model because the α_t values, in general, increase with the molecular weight of the permeating molecule as would be predicted by this model. It is of interest to note that the fluxes are higher, and the α_t values smaller, for the CP200 membrane than for the BP20 membrane. This trend is consistent with the nearly universal observation that membranes that show higher fluxes show lower selectivities.[39,40] One possible explanation for this result is that the ODS completely fills portions of the nominally 20-nm-diameter pores in the BP20 membrane, creating a highly hydrophobic region within the mouth of the pore. This would not be possible in the much larger diameter pores of the CP200 membrane.

Elucidating the Transport Mechanism. The experiments discussed above demonstrate that the transport mechanism for a homologous series of nonionic permeating molecules in the ODS-modified membranes involves hydrophobic-effect-based partitioning of the molecule into the membrane. However, at least two different mechanisms involving hydrophobic-effect-based partitioning can be proposed. The first assumes that the partition process is akin to the solvent extraction of a hydrophobic molecule from water into an immiscible nonpolar solvent.[41] The second assumes that the partition process is analogous to Langmuir adsorption of a hydrophobic molecule from water onto a hydrophobic surface.[42,43] We develop here equations that describe each of these mechanisms and present results of experiments that have allowed us to determine which of these mechanism is operative in the ODS-modified membranes.

Both mechanisms entail Fick's first law of diffusion, which for a linear concentration gradient across the membrane can be written as

$$J_x = D\frac{\Delta C}{L} \tag{3}$$

where J_x is the flux of a permeating molecule (X) through the membrane, D is the diffusion coefficient for X in the membrane, ΔC is the concentration gradient of X across the membrane, and L is the membrane thickness. In the solvent-extraction

mechanism, the partitioning of X into the membrane is described by[41]

$$X_{aq} \rightarrow X_{memb} \tag{4}$$

And the partition coefficient, K_P, is given by

$$K_p = \frac{[X_{memb}]}{[X_{aq}]} \tag{5}$$

In our experiments, $[X_{aq}]$ is the concentration of X in the feed solution, C_{feed}. Substituting this into eq 5 and rearranging yields

$$[X_{memb}] = K_p C_{feed} \tag{6}$$

The concentration of X in the membrane on the feed-solution side is this $[X_{memb}]$, and the concentration of X in the membrane on the receiver-solution side is always effectively zero. This makes the concentration gradient to be used in eq 3 $\Delta C = [X_{memb}] = K_P C_{feed}$, and eq 3 becomes

$$J_x = DK_p \frac{C_{feed}}{L} \tag{7}$$

According to eq 7, the flux for this solvent-extraction-based transport mechanism is linearly related to C_{feed}, the concentration of the permeating molecule X in the feed solution.

The alternative transport mechanism assumes that partitioning into the membrane is described by the Langmuir-adsorption isotherm, which can be written as,[42,43]

$$[X_{memb}] = \frac{C_{max} K_L C_{feed}}{1 + K_L C_{feed}} \tag{8}$$

where C_{max} is the saturation concentration of X in the membrane, and K_L is the Langmuir-adsorption constant. For the ODS-modified membranes, K_L describes the hydrophobic-effect-driven adsorption of X from the aqueous feed solution onto the hydrophobic ODS layers lining the pore walls in the membrane. Substituting eq 8 into eq 3, and recalling that $\Delta C = [X_{memb}]$, gives

$$J_x = \frac{D}{L}\left(\frac{C_{max} K_L C_{feed}}{1 + K_L C_{feed}}\right) \tag{9}$$

Equation 7 (solvent-extraction mechanism) predicts that a plot of flux vs C_{feed} will be linear, whereas eq 9 (Langmuir-adsorption mechanism) predicts that this plot will have a shape characteristic of a Langmuir-adsorption isotherm,[42,43] i.e., a linear increase of flux with C_{feed} at low C_{feed} values, followed by a plateau at higher C_{feed} values. Transport experiments with phenol as the permeating species, and ODS-modified BP20 membranes, were used to explore the flux vs C_{feed} relationship. Phenol was chosen for these studies because it has the highest water solubility (maximum solubility ~825 mM[44]) of the permeating molecules studied here; this allowed us to explore the flux vs C_{feed} relationship over the largest possible range of C_{feed} values.

In agreement with the Langmuir-adsorption mechanism, the experimental plot of flux vs C_{feed} for phenol transport shows a linear portion at low C_{feed} values followed by a plateau at higher

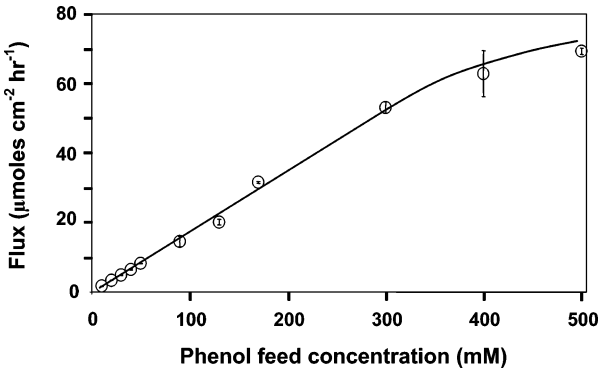

Figure 4. Plot of flux vs feed concentration for phenol transport in an ODS-modified BP20 membrane.

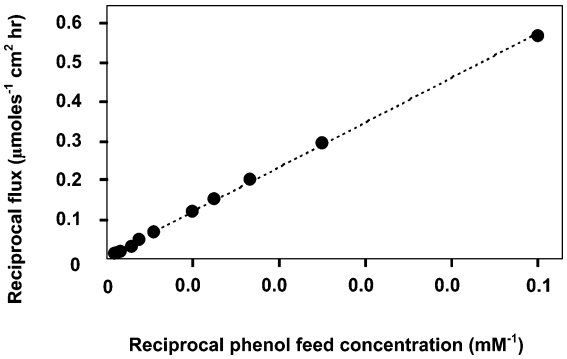

Figure 5. Plot as per eq 10 for phenol transport in an ODS-modified BP20 membrane.

C_{feed} values (Figure 4). This plot can be linearized by rearranging eq 9 to yield

$$J_X^{-1} = \left(\frac{L}{DC_{max}K_L}\right)\frac{1}{C_{feed}} + \frac{L}{DC_{max}} \tag{10}$$

According to eq 10, a plot of $1/J_x$ vs $1/C_{feed}$ will be linear, with slope equal to $L/(DC_{max}\ K_L)$ and y-intercept equal to $L/(DC_{max})$. Figure 5 shows that this plot is, indeed, linear (correlation coefficient = 0.9995), and dividing the y-intercept (0.004 ± 0.002 μmol cm^{-2} h^{-1}) by the slope (5.71 ± 0.06 μmol cm^2 h^{-1} mM) gives $K_L = 7 \times 10^{-4}$ mM^{-1} for the adsorption of phenol on the hydrophobic ODS layers lining the pore walls in the BP20 membrane.

Figure 4 shows that the experimental flux vs C_{feed} data follow the Langmuir-adsorption mechanism up to a feed concentration of 500 mM, and that the plateau flux is approximately 80 μmol cm^{-2} h^{-1}. We found, however, that the flux increased to 500 ± 100 μmol cm^{-2} h^{-1} for a phenol feed concentration of 700 mM. This dramatic increase in flux is not predicted by either the Langmuir-adsorption or solvent-extraction mechanisms. It occurred to us that this anomalously high phenol flux might reflect a change in the wetting properties of the aqueous feed solution such that, at this very high concentration of phenol (700 mM), the feed solution now floods the pores in the ODS-modified membrane. To explore this issue, transport experiments were conducted on an ODS-modified BP20 membrane by using a feed solution that was 700 mM in phenol and 100 mM in Ni^{2+}. As shown above, if the pores are not wetted by the feed solution, Ni^{2+} cannot be transported across the membrane; however, Ni^{2+} transport does occur when the feed solution is 700 mM in phenol. These data show that the anomalously high phenol flux at this C_{feed} value is caused by flooding of the pores.

Supported-Liquid Membranes. The Langmuir-adsorption-induced plateau in permeated flux at high feed concentrations

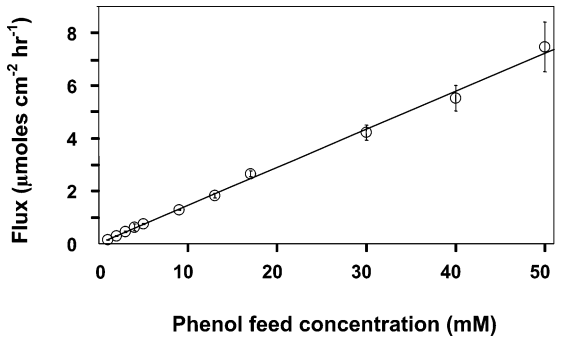

Figure 6. Plot of flux vs feed concentration for phenol transport in the mineral-oil-based supported-liquid membrane.

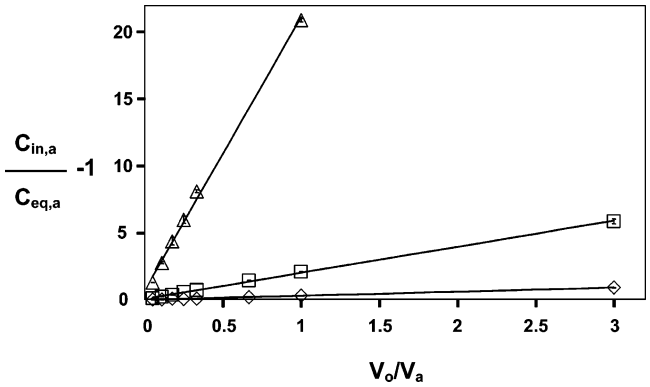

Figure 7. Mineral-oil/water solvent-extraction data plotted as per eq 2 for (△) TMP, (□) DMP, and (◇) PC.

(Figure 4) is undesirable because it limits the range of concentrations over which optimal transport selectivity will be observed. Because this plateau would not be observed if the solvent-extraction mechanism were operative (eq 7), it would advantageous if the membranes could be forced to follow the solvent-extraction mechanism. This can be accomplished by creating a subphase of a water-immiscible liquid within the pores of the ODS-modified BP20 membrane, a supported-liquid membrane.[30,31] Supported-liquid membranes based on light mineral oil, a mixture of hydrocarbons ranging from 18 to 35 carbons, were investigated here.

Figure 6 shows the phenol flux vs feed-concentration plot for a mineral-oil-based supported-liquid membrane. In contrast to the membranes that did not contain this water-immiscible liquid within the pores (Figure 4), the plot for the supported-liquid membrane is linear over the entire feed-concentration range investigated. These data clearly show, as expected, that the supported-liquid membrane follows the solvent-extraction mechanism (eq 7) rather than the Langmuir-adsorption mechanism (eq 9).

Because of the importance of the partition coefficients in determining both the rate and selectivity of transport for the supported-liquid membrane (eq 7), we have measured the mineral-oil/water partition coefficients for the various permeating molecules studied here. Plots of $[(C_{in,a}/C_{eq,a}) - 1]$ vs V_o/V_a (eq 2)[34,35] for partitioning of TMP, DMP, and PC between mineral oil and water are shown in Figure 7; analogous data were obtained for phenol as well. The K_p values obtained from the slopes of these plots are shown in Table 3. As would be expected, the partition coefficient increases with the hydrophobicity of the partitioning molecule.

We have defined the transport selectivity coefficient (α_t) as the flux of a permeating molecule in a particular membrane divided by the phenol flux in that membrane. For the solvent-extraction mechanism, α_t is the product of DK_p for the permeating molecule in the membrane divided by DK_p for phenol in that membrane (eq 7). Hence, the partition coefficient ratio is an important factor in determining the transport selectivity. These partition coefficient ratios (defined as α_p, where the subscript p denotes partition selectivity coefficient) are also shown in Table 3. These partition selectivity coefficients can be quite large, and the key question now is: are the measured transport selectivity coefficients for the supported-liquid membranes correspondingly large?

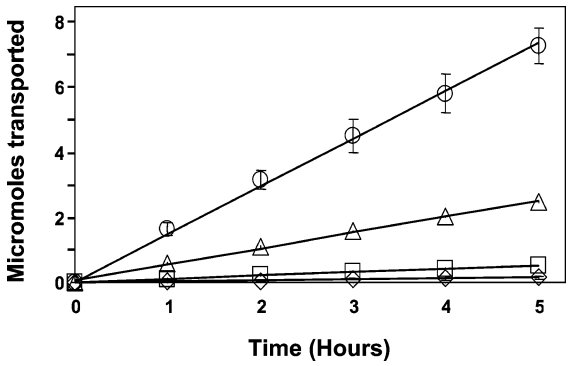

Figure 8. Flux plots for the mineral-oil-based supported-liquid membrane, (○) TMP, (△) DMP, (□) PC, (◇) Ph. The feed concentration was 2 mM.

TABLE 3: Mineral-Oil/Water Partition Coefficients (K_p) and Partition Selectivity Coefficients (α_p)

molecule	K_p	α_p
Ph	0.12 ± 0.01	1
PC	0.304 ± 0.003	2.6
DMP	1.95 ± 0.02	17
TMP	20.4 ± 0.4	180

TABLE 4: Fluxes and Transport Selectivity Coefficients (α_t) for the Various Permeating Species in the Mineral-Oil-Based Supported-Liquid Membrane; Feed Concentration Was 2 mM.

permeating molecule	flux (μmol cm^{-2}h^{-1})	α_t
Ph	0.032 ± 0.003	1
PC	0.108 ± 0.003	3.3
DMP	0.50 ± 0.01	16
TMP	1.48 ± 0.03	46

Flux plots for the homologous series of permeating molecules through the mineral-oil-based supported-liquid membrane are linear (Figure 8), and the fluxes and transport selectivity coefficients obtained from these plots are shown in Table 4. We see that the transport selectivity coefficients for PC and DMP (Table 4) are essentially identical to the corresponding partitioning selectivity coefficients (Table 3). Because α_t is the ratio of the product DK_p, these data show that the D values for Ph, PC, and DMP in the mineral oil subphase are, to our ability to make the measurement, identical. Given the small differences in the sizes of these various molecules (vide infra), this is not surprising.

In contrast to Ph, PC, and DMP, the transport selectivity coefficient for TMP (Table 4) is a factor of 4 times smaller than the partitioning selectivity coefficient (Table 3). Part of the reason for this discrepancy is that the diffusion coefficient for the larger TMP molecule in mineral oil is less than that for phenol. However, as we will see below, the difference in the diffusion coefficients for phenol vs TMP is too small to account for the factor of 4 discrepancy between α_t and α_p. While we cannot at this time account for the discrepancy, it is important

TABLE 5: Permeation Data for the ODS-Modified BP20 Membrane[a]

molecule	K_L (mM^{-1})	D ($cm^2\ sec^{-1}$)	α_D	α_{SE}	molecular radius (nm)[b]	molecular surface area (nm^2)[b]
Ph	7.00E−04	1.22E−06	1.000	1.000	0.293	1.17
PC	0.0018	6.80E−07	0.557	0.970	0.301	1.36
DMP	0.0114	2.10E−07	0.172	0.890	0.330	1.56
TMP	0.117	4.31E−08	0.035	0.820	0.359	1.76

[a] Langmuir-adsorption constants (K_L), diffusion coefficients (D), diffusion selectivity coefficients (α_D), diffusion selectivity coefficients calculated from the Stokes−Einstein equation (α_{SE}), and calculated radii and surface areas for each of the permeating molecules. [b] See Experimental Section for details.

to note that the transport selectivity coefficients for this supported-liquid membrane are much higher than the analogous selectivity coefficients obtained for the other membranes studied here.

Diffusion Coefficients for the Permeating Molecules in the ODS-Modified BP20 Membrane. In the ODS-modified membranes that do not contain the mineral oil subphase, transport occurs by diffusion of the permeating molecule along the ODS layers coating the walls of the nonwater-wetted pores. We describe here a method for determining the diffusion coefficient associated with this transport process. To show how this is accomplished, it is important to point out that implicit in the Langmuir-adsorption process is the concept that the adsorbing molecule binds to a limited number of sites on the surface. The concentration of these adsorption sites is the parameter C_{max} (eqs 8−10), and in order to calculate the diffusion coefficients, we must obtain a value for this parameter in the ODS-modified BP20 membrane.

At low feed concentrations, where the product $K_L C_{feed} \ll 1$, eq 8 simplifies to

$$[X_{memb}] = C_{max} K_L C_{feed} \tag{11}$$

By comparing eq 11 (Langmuir mechanism) to eq 6 (solvent-extraction mechanism), we see that the partition coefficient, K_p, is related to K_L via

$$K_p = C_{max} K_L \tag{12}$$

Equation 12 allows us to calculate C_{max} for the ODS-modified membranes, provided we have values for both K_p and K_L for one of the permeating molecules in this membrane.

While the transport data for phenol in the ODS-modified BP20 membrane gave $K_L = 7 \times 10^{-4}\ mM^{-1}$, we do not have an experimental K_p associated with the partitioning of phenol between water and ODS. We do, however, have an experimental K_p value for partitioning of phenol between water and mineral oil (Table 3), and while the data are not shown, the K_p value for partitioning of phenol between water and kerosene is identical to the mineral-oil/water value. Because kerosene contains hydrocarbons of 9−16 carbons[45] and mineral oil contains hydrocarbons of 18−35 carbons,[46] there is no question that K_p for partitioning of phenol between water and ODS (18 carbons) is identical to the $K_p = 0.12$ obtained for both mineral oil and kerosene. Using this K_p and $K_L = 7 \times 10^{-4}\ mM^{-1}$ in eq 12 gives a C_{max} value for phenol in the ODS-modified BP20 membrane of 171 mM.

While C_{max} was experimentally determined for only phenol, it is clear that the other permeating molecules bind to the same sites in the membrane as does phenol. This is true because the adsorption mechanism is the same for all of the members of this homologous series of molecules. Hence, to a first approximation, C_{max} will be the same for all of the molecules in this homologous series. This value of C_{max} was used with the K_p values in Table 3 to calculate (eq 12) K_L for PC, DMP, and TMP (Table 5). These K_L values (and the value for C_{max}) allow us to use eq 9 and the experimental fluxes for the ODS-modified BP20 membrane (Table 2) to calculate diffusion coefficients for all of the permeating molecules in this membrane.

These diffusion coefficients, along with the diffusion coefficient ratios (α_D, relative to phenol), are shown in Table 5. Table 5 also shows diffusion coefficient ratios (again relative to phenol) calculated from the Stokes−Einstein equation[29] and the radii and surfaces areas of each molecule. The Stokes−Einstein ratios are important because they show how the diffusion coefficients would vary with the size of the permeating molecule if the molecule were diffusing in solution. We see from Table 5 that the experimental diffusion-coefficient ratios (α_D) are less than the Stokes−Einstein ratios (α_{SE}), and that the differences between these ratios increase with the size of the permeating molecule. These data unambiguously show that the simple Stokes−Einstein solution-based diffusion model does not apply to the ODS-modified BP20 membrane. This is not surprising because the pores in this membrane are devoid of water, and transport occurs along the ODS layers coating the pore walls.

If the Stokes−Einstein model were applicable, D would scale inversely with the molecular radius. In contrast, the D values for the ODS-modified PB20 membrane scale inversely with molecular area (slope $= 4 \times 10^{-20}\ cm^4\ s^{-1}$, correlation coefficient $= 0.987$). We propose that this inverse molecular-area dependence is a signature for a solid-state diffusion process.[47] This greater sensitivity to molecular size has dire consequence for the selectivity of membranes that use the Langmuir-adsorption transport mechanism. This is because, for a small molecule, K_L will be small but D will be large, whereas for a large molecule, K_L might be large but D (as indicated in Table 5) will be very small. As a result, as clearly shown by the experimental data in Table 2, the transport selectivity of such membranes will, in general, be worse than for membranes where transport occurs in a liquid subphase (Table 4).

Conclusions

We have shown that the transport properties of nanopore alumina membranes can be tailored by chemically functionalizing the membrane. When functionalized with ODS, the pores in the membrane become so hydrophobic that they are not wetted by water. Nonionic molecules can nevertheless be transported from an aqueous feed solution on one side of the membrane to an aqueous receiver solution on the other side. The transport mechanism involves Langmuir-type adsorption of the permeating molecule onto the ODS layers lining the pore walls and solid-state diffusion along these ODS layers.

When a homologous series of permeating molecules is used, flux across the membrane increases with the hydrophobicity of the molecule. This is because the Langmuir-adsorption constant onto the ODS increases with the hydrophobicity of the molecule.

However, these ODS-modified membranes show poor transport selectivity for hydrophobic permeating molecules (Table 2). As discussed above, this is an unfortunate consequence of the solid-state diffusion process that is responsible for transporting the molecule across the membrane. Transport selectivity can be dramatically improved by filling the pores of the ODS-modified membrane with the water-immiscible (hydrophobic) liquid mineral oil (Table 4). Selectivity improves for these supported-liquid membranes because the liquid-phase (as opposed to solid-state) diffusion coefficient is not as strongly attenuated with increasing size of the permeating molecule.

Finally, eq 7, which describes how flux varies with the partition coefficient, K_p, and diffusion coefficient, D, could prove useful for predicting the flux of a particular molecule across the supported-liquid membrane. This is because partition coefficients can be calculated from the molecular structure,[48,49] and the diffusion coefficient can be calculated from the Stokes−Einstein equation.[29]

Acknowledgment. This work was supported by the Department of Energy and the National Science Foundation.

References and Notes

(1) Wu, J. C.; Cheng, L. C. *J. Membr. Sci.* **2000**, *167*, 253−261.
(2) Gowman, L. M.; Ethier, C. R. *J. Membr. Sci.* **1997**, *131*, 107−123.
(3) Maoddeb, M.; Koros, W. J. *J. Membr. Sci.* **1997**, *125*, 143−163.
(4) Ghayeni, S.; Beatson, P. J.; Fane, A. J.; Schneider, R. P. *J. Membr. Sci.* **1999**, *153*, 71−82.
(5) Herath, G.; Yamamoto, K.; Urase, T. *Water Sci. Technol.* **1998**, *38*, 489−496.
(6) Martin, C. R. *Science (Washington, D.C.)* **1994**, *266*, 1961−1966.
(7) Schönenberger, C.; van der Zande, B. M. I.; Fokkink, L. G. J.; Henny, M.; Schmid, C.; Krüger, M.; Bachtold, A.; Huber, R.; Birk, H.; Staufer, U. *J. Phys. Chem. B* **1997**, *101*, 5497−5505.
(8) Nicewarner-Peña, S. R.; Freeman, R. G.; Reiss, B. D.; He, L.; Peña, D. J.; Walton, I. D.; Cromer, R.; Keating, C. D.; Natan, M. J. *Science (Washington, D.C.)* **2001**, *294*, 137−141.
(9) Ilic, R.; Skvarc, J.; Golovchenko, A. N. *Radiat. Meas.* **2003**, *36*, 83−88.
(10) Apel, P. *Nucl. Instrum. Methods Phys. Res., Sect. B* **2003**, *208*, 11−20.
(11) Fleischer, R. L.; Price, P. B.; Walker, R. M. *Nuclear Tracks in Solids. Principles and Applications*; University of California Press: Berkeley, CA, 1975; p 605.
(12) Jessensky, O.; Müller, F.; Gösele, U. *Appl. Phys. Lett.* **1998**, *72*, 1173−1175.
(13) Thompson, G. E.; Wood, G. C.; Furneaux, R. C. *Corros. Sci.* **1978**, *18*, 481−498.
(14) Martin, C. R.; Kohli, P. *Nat. Rev. Drug Discovery* **2003**, *2*, 29−37.
(15) Hou, S.; Wang, J.; Martin, C. R. *Nano Lett.* **2005**, *5*, 231−234.
(16) Wirtz, M.; Martin, C. R. *Adv. Mater.* **2003**, *15*, 455−458.
(17) Wirtz, M.; Parker, M.; Kobayashi, Y.; Martin, C. R. *Chem.—Eur. J.* **2002**, *16*, 3572−3578.
(18) Chakarvarti, S. K.; Vetter, J. *Radiat. Meas.* **1998**, *29*, 149−159.
(19) Jirage, K. B.; Hulteen, J. C.; Martin, C. R. *Science (Washington, D.C.)* **1997**, *278*, 655−658.
(20) Yu, S.; Lee, S. B.; Martin, C. R. *Anal. Chem.* **2003**, *75*, 1239−1244.
(21) Martin, C. R.; Nishizawa, M.; Jirage, K.; Kang, M.; Lee, S. B. *Adv. Mater.* **2001**, *13*, 1351−1361.
(22) Kohli, P.; Harrell, C. C.; Cao, Z.; Gasparac, R.; Tan, W.; Martin, C. R. *Science (Washington, D.C.)* **2004**, *305*, 984−986.
(23) Smuleac, V.; Butterfield, D. A.; Bhattacharyya, D. *Chem. Mater.* **2004**, *16*, 2762−2771.
(24) Chun, K.; Stroeve, P. *Langmuir* **2002**, *18*, 4653−4658.
(25) Hou, Z.; Abbott, N. L.; Stroeve, P. *Langmuir* **2000**, *16*, 2401−2404.
(26) Steinle, E. D.; Mitchell, D. T.; Wirtz, M.; Lee, S. B.; Young, V. Y.; Martin, C. R. *Anal. Chem.* **2002**, *74*, 2416−2422.
(27) Jirage, K. B.; Hulteen, J. C.; Martin, C. R. *Anal. Chem.* **1999**, *71*, 4913−4918.
(28) Hulteen, J. C.; Jirage, K. B.; Martin, C. R. *J. Am. Chem. Soc.* **1998**, *120*, 6603−6604.
(29) Bockris, J. O. M.; Reddy, A. K. N. *Modern Electrochemistry*; Plenum Publishing: New York, 1970; p 380.
(30) Chimuka, L.; Mathiasson, L.; Jönsson, J. *Anal. Chim. Acta* **2000**, *416*, 77−86.
(31) Farrell, S.; Sirkar, K. K. *J. Controlled Release* **1999**, *61*, 345−360.
(32) Wu, J. C.; Lee, E. *J. Membr. Sci.* **1999**, *154*, 251−259.
(33) Kuwabata, S.; Martin, C. R. *J. Membr. Sci.* **1994**, *91*, 1−12.
(34) Brookes, P. R.; Livingston, A. G. *J. Membr. Sci.* **1995**, *104*, 119−137.
(35) Han, S.; Puech, L.; Law, R. V.; Steinke, J. H. G.; Livingston, A. *J. Membr. Sci.* **2002**, *199*, 1−11.
(36) Miller, S. A.; Martin, C. R. *J. Am. Chem. Soc.* **2004**, *126*, 6226−6227.
(37) Paul, K. C. *Org. Biomol. Chem.* **2005**, *3*, 1176−1179.
(38) Groisman, L.; Rav-Acha, C.; Gerstl, Z.; Mingelgrin, U. *Appl. Clay Sci.* **2004**, *24*, 159−166.
(39) Robeson, L. M. *J. Membr. Sci.* **1991**, *62*, 165−185.
(40) Freeman, B. D. *Macromolecules* **1999**, *32*, 375−380.
(41) Berthod, A.; Broch, S. C. *J. Chromatogr., A* **2004**, *1037*, 3−14.
(42) Langmuir, I. *J. Am. Chem. Soc.* **1916**, *38*, 2221−2295.
(43) Paul, D. R.; Koros, W. J. *J. Polym. Sci., Polym. Phys. Ed.* **1976**, *14*, 675−685.
(44) Jaoui, M.; Achard, C.; Rogalski, M. *J. Chem. Eng. Data* **2002**, *47*, 297−303.
(45) Gómez-Carracedo, M. P.; Andrade, J. M.; Fernandez, E.; Prada, D.; Muniategui, S. *Fuel* **2003**, *82*, 1211−1218.
(46) Grob, K.; Vass, M.; Biedermann, M.; Neukom, H. P. *Food Addit. Contam.* **2001**, *18*, 1−10.
(47) Politzer, P.; Murray, J. S.; Flodmark, P. *J. Phys. Chem.* **1996**, *100*, 5538−5540.
(48) Leo, A.; Hansch, C. *J. Org. Chem.* **1971**, *36*, 1539−1544.
(49) Leo, A.; Hansch, C.; Elkins, D. *Chem. Rev.* **1971**, *71*, 525−616.